

Reduction of Radiative Heat Loss in Small Modular Reactors Through Thermal Radiation Shielding: An Experimental and CFD Approach

Beomjin Jeong^a, Geunyoung Byeon^a, Namgook Kim^a, and Sung Joong Kim^{a, b*}

^a Department of Nuclear Engineering, Hanyang Univ., 222 Wangsimni-ro, Seongdong-gu, Seoul, Korea

^b Institute of Nano Science and Technology, Hanyang University., 222 Wangsimni-ro, Seongdong-gu, Seoul, Korea

*Corresponding author: sungkim@hanyang.ac.kr

***Keywords:** small modular reactor, metal containment vessel, thermal radiation shielding, heat loss mechanism, radiative heat transfer

1. Introduction

Small Modular Reactors (SMRs) offer a promising alternative to large-scale nuclear plants, owing to their enhanced safety features, reduced capital costs, and flexibility in deployment. Many SMR concepts, however, diverge from conventional reactor designs by incorporating metallic containment vessels (MCVs) rather than the steel-reinforced concrete structures typical of pressurized water reactors. Although the elevated thermal conductivity of metals improves heat dissipation during accident scenarios [1], it can also intensify unwanted heat losses under normal operating conditions, especially in the absence of external insulation.

Several SMRs, including the Korean “innovative-SMR” (i-SMR), adopt a vacuum or low-pressure gap between the reactor pressure vessel (RPV) and the MCV. Under moderately high temperatures of 300–330 °C and near-vacuum environments (0.07–0.1 bar), convective heat transfer diminishes, making radiation the dominant energy transport mechanism. Historically, radiation has received less attention than conduction and convection in the context of reactor heat removal. Recent experimental and computational studies, however, confirm that disregarding radiation leads to a substantial underestimation of heat losses [2].

To address this issue, researchers have proposed installing thermal radiation shields (TRSs)—thin metallic cylinders with low emissivity—between the RPV and the containment boundary. By intercepting radiative emissions and re-emitting only a fraction of that energy, these shields can significantly lower overall heat loss (Figure 1) [3]. Materials like polished aluminum, with an emissivity around 0.04, are particularly promising compared to stainless steel, which exhibits higher emissivity. The performance of a TRS depends not only on the material’s emissivity but also on its diameter, placement, and surface condition.

This paper presents a study on TRSs in a scaled SMR environment, involving both experimental tests and computational fluid dynamics (CFD) simulations. An experimental apparatus was built to replicate the key geometry and boundary conditions of the i-SMR design. Test cases ranged from no shielding to multiple shield configurations in aluminum (varying diameters) and

stainless steel. The experimental data were then compared with CFD predictions to validate the observations and to elucidate heat transfer paths under vacuum condition. By integrating experimental findings with numerical analysis, this work provides a detailed assessment of TRS effectiveness in mitigating radiative heat losses, thereby offering practical insights for optimizing SMR containment designs.

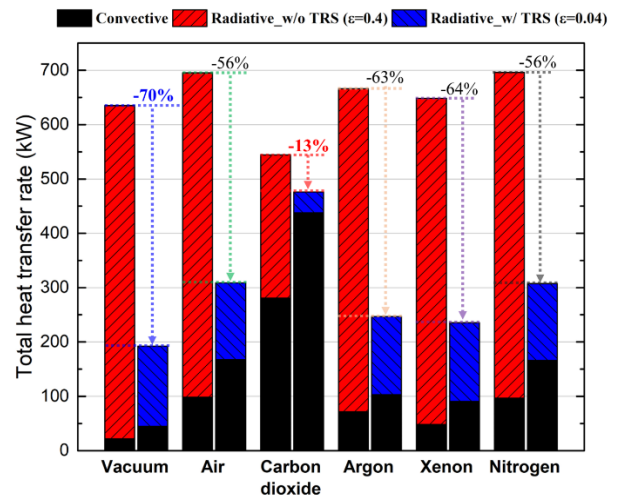


Fig. 1. Comparison of the heat loss with and without thermal radiation shielding (TRS) [3].

2. Experimental Methodology

2.1 Experimental Setup

An experimental apparatus was constructed to mimic the thermal environment surrounding an SMR’s reactor pressure vessel (RPV) (Figure 2). This apparatus consists of two concentric cylindrical components: an inner heater assembly and an outer stainless-steel chamber. The gap between these cylinders can be evacuated or maintained at a low pressure (~0.07–0.08 bar), reflecting the vacuum gap concept often adopted in SMRs.

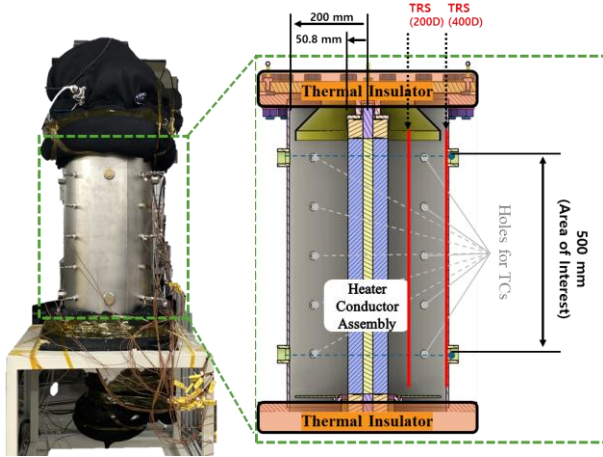


Fig. 2. The experimental apparatus and area of interest.

At the heart of the apparatus is a cartridge heater capable of delivering up to 4.5 kW. During operation, it provided power to sustain a conductor surface temperature of approximately 320 °C. The conductor itself is made of aluminum, chosen for its high thermal conductivity, and dimensioned in proportion to the SMR's pressurizer region. By calibrating the conductor's size, the view factor — i.e., the fraction of radiative energy reaching the chamber — remains within roughly $\pm 10\%$ of that observed in the actual reactor design.

The outer stainless-steel chamber envelops the conductor and is sealed at both the top and bottom using flanges, enabling precise control of the internal pressure. Ceramic-fiber insulation lines regions outside the main gap to limit extraneous conduction effects.

To investigate methods for reducing radiative heat loss, thin Thermal Radiation Shields (TRSs) with low emissivity were incorporated. Two materials (aluminum and SS304) were tested, each available in 200 mm and 400 mm diameters. The smaller-diameter shield was placed about one-third of the radial gap from the conductor, whereas the larger diameter option was positioned closer to the chamber wall. Both shields were mounted on Polyether Ether Ketone (PEEK) supports to reduce conductive contact and thereby minimize additional heat transfer pathways.

2.2 Instrumentation and Measurements

Multiple K-type thermocouples (0.1 mm diameter) were embedded at various radial depths in the conductor and in the chamber wall to capture temperature profiles. Additional thermocouples aligned vertically monitored axial temperature gradients. A vacuum gauge at the top flange tracked chamber pressure, and a nearby RTD measured ambient conditions. Heater voltage and current were monitored using a DC power supply with specified accuracies of ± 0.45 V and ± 0.05 A, respectively. All sensor data were logged at one-second intervals via a data acquisition

system. Figure 3 shows the schematic of experimental apparatus for i-SMR.

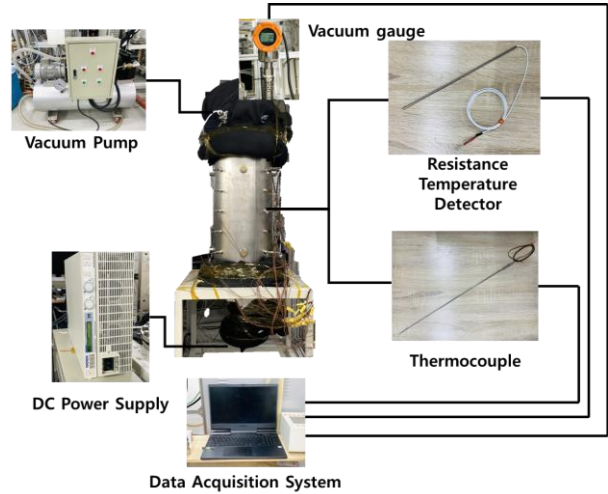


Fig. 3. Schematic of experimental apparatus for i-SMR.

2.3 Test Matrix

Five test configurations were established:

- Background Conduction:** Filling the gap with ceramic fiber to suppress radiation and convection.
- Base Case (No Shield):** Evacuated gap (~ 0.07 bar), no TRS.
- Al-200:** A 200 mm-diameter aluminum shield, installed one-third of the way from the conductor.
- Al-400:** A 400 mm-diameter aluminum shield, positioned near the chamber wall.
- SS304-400:** A similarly sized (400 mm) stainless-steel shield, to compare with aluminum's lower emissivity.

Through these comparisons, the influence of shield presence, material, and dimension on total heat loss was determined. Table 1 summarizes the test matrix designed to evaluate the thermal insulation performance of the TRSs.

Table 1: Test matrix for evaluating the thermal insulation performance of the TRS

Experimental Cases	Filling condition (pressure)	TRS parameters	
		Material	Diameter (mm)
Background conduction case (w/o TRS)	Ceramic Fiber Insulator (0.07 bar)	-	-
Base case (w/o TRS)	Vacuum (0.07 bar)	-	-
Al-200	Vacuum (0.07 bar)	Aluminum	200
Al-400	Vacuum (0.07 bar)	Aluminum	400
SS304-400	Vacuum (0.07 bar)	SS304	400

2.4 Experimental Procedure

Before each run, the apparatus was purged with air and gradually drawn down to about 0.07–0.08 bar. The heater was then activated, and any pressure rises were managed by intermittent pumping. A steady state was declared once conductor and chamber temperatures varied by less than 0.5 °C over a 3,600-second window. If the conductor surface did not stabilize at ~320 °C, heater power was raised incrementally until it did. Final readings were collected over an additional 30-minute span, ensuring consistent steady-state data.

3. Numerical Analysis

3.1 CFD Model Description

A two-dimensional axisymmetric CFD model was developed in ANSYS FLUENT to reflect the cylindrical geometry of the experimental apparatus. This simplified approach avoids the computational overhead of a full 3D model and is justified by the negligible azimuthal variations expected under near-vacuum conditions.

3.2 Geometry and Mesh Generation

A cross-sectional mesh was generated from the apparatus dimensions, with finer grids near steep temperature gradients (e.g., around the heater) and coarser meshes in insulated regions. A mesh independence study confirmed that total heat flux stabilized with approximately 700k–800k elements. Figure 4 shows the appearances of the mesh for each geometry.

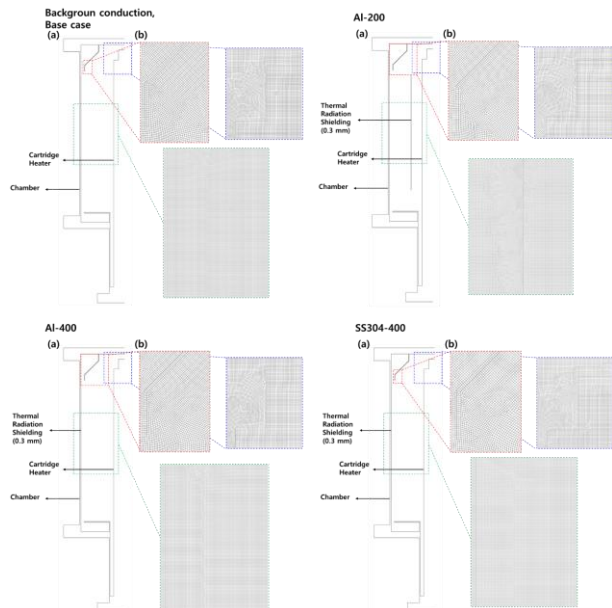


Fig. 4. (a) The two-dimensional axisymmetric geometry of the experimental apparatus and (b) the mesh created from geometry.

3.3 Model Setup and Solver Configuration

Boundary conditions were set to replicate the experimental scenario: the aluminum conductor was fixed at 320 °C, while the ambient boundary was ~18 °C (Figure 5). The gap was assigned properties consistent with low-pressure air. Although convection is minimal under near-vacuum conditions, the $k-\omega$ Shear Stress Transport model was used to capture any transitional flow. Radiative heat transfer was treated using the Discrete Ordinates (DO) model with a 5×5 angular discretization per octant, employing nominal emissivity values for the conductor, chamber, and shields. A gray radiation assumption was adopted to simplify wavelength-dependent effects. Table 2 summarizes the physical property values of the materials.

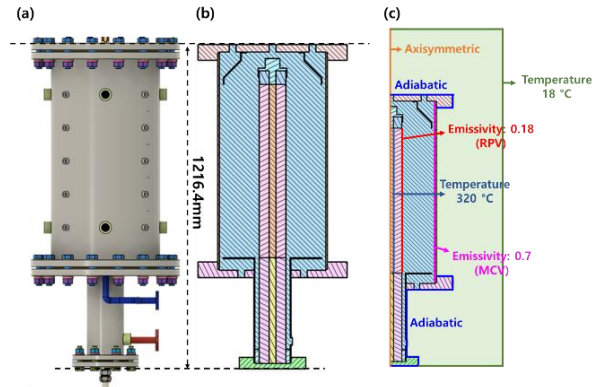


Fig. 5. (a) Experimental apparatus geometry, (b) Geometry cross-section based on the experimental apparatus, and (c) Setting up boundary conditions for a CFD analysis.

Table 2: Materials and physical properties for CFD analysis [3, 4, 5].

Material	ρ [kg/m ³]	μ [kg/m·s]	k [W/m·K]	c_p [J/kg·K]	ϵ
Vacuum	0.17281 -3.97733E-4 (T) +2.97726E-7 (T ²)	2.5113E-5	0.03674	1020.5	-
Al Conductor	2719		202.4	871	0.18
Al TRS					0.04 (Polished)
SS304 Chamber	7990		16.3	500	0.7 (Anodizing)
SS304 TRS					0.3 (Lightly oxidized)
Insulator	145		0.1	780	1
PEEK	1183		0.22	0.32	1

All simulations used a pressure-based solver with SIMPLE coupling. Second-order upwind schemes discretized the momentum and energy equations, with convergence deemed acceptable once continuity, energy, and turbulence residuals dropped below 1.0E-6. Radiative flux residuals had to meet a similar criterion. Final heat flux values were computed from surface boundary integrals and compared against experimental measurements for validation. The information about the

models and solvers used for analyzing heat transfer mechanisms is summarized in Table 3.

Table 3: About the analysis models and solver selected to simulate key phenomena.

Viscous Models		k-omega SST
Radiation Models		Discrete Ordinates (Gray)
Spatial Discretization	Gradient	Least Squares Cell Based
	Pressure	Body Force Weighted
	Momentum	2nd Order Upwind
	Energy	2nd Order Upwind
Pressure-based solver		SIMPLE

4. Results and Discussion

4.1 Experimental Observations

Five test configurations were examined (Background Conduction, Base, Al-200, Al-400, SS304-400) to quantify heat loss under various shielding scenarios (Table 4). In the *Background Conduction* case, ceramic fiber filling the gap yielded the lowest heat loss (~144 W), as conduction alone dominated. By contrast, the *Base case* (no shield at ~0.07 bar) saw heat loss climb to ~339 W, with ~60% of that attributed to radiation.

Table 4: The results of the experiments for the TRS.

Experimental Case	Heater Temp. (°C)	Chamber Pressure (bar)	Ambient Temp. (°C)	Heater Input (W)
Background conduction case	320.40	0.08	18.08	144.34
Base case	319.97	0.05	18.52	338.53
Al-200	319.87	0.06	17.86	289.11
Al-400	320.13	0.06	17.60	297.03
SS304-400	320.04	0.06	18.31	327.38

○ The Insulation Performance of Thermal Radiation Shields

Introducing a 400 mm aluminum shield (Al-400) reduced heat loss by ~12% relative to the Base, and further testing revealed that a 200 mm aluminum shield (Al-200) was ~3% more effective than the larger diameter. Experiments also showed that stainless steel (SS304) resulted in about 10% higher heat loss compared to aluminum, underscoring the impact of lower emissivity materials. The lowest heat loss overall was recorded for Al-200, while SS304-400 showed the highest.

○ Heat Loss Mechanism at the Area of Interest

The heater input power accounts for total heat dissipation—including insulated sections—but the analysis focused on the non-insulated region where radiative heat dominates under near-vacuum conditions. Measurements indicated that, without a shield, most radiation from the conductor reached the chamber walls, whereas an aluminum TRS effectively blocked or reradiated less energy due to its low emissivity (~0.04). Consequently, Al-200 produced the least radiative heat transfer. The results of the radiative heat transfer from the conductor to the area of interest are presented in Figure 6.

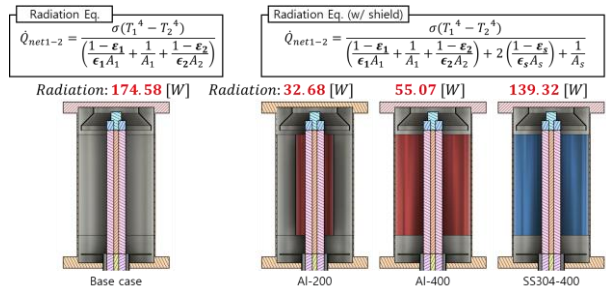


Fig. 6. The calculation formula and calculation results for the radiative heat transfer from the conductor to the area of interest.

Estimations of chamber-to-ambient heat loss (using a nominal convective heat transfer coefficient of 7 W/m²·K) corroborated these trends: the Base case reported the highest heat loss, while Al-200 consistently achieved the lowest. Although discrepancies arose from assumptions (e.g., emissivity and flange conduction), the overall results highlight that lower-emissivity TRSs, coupled with careful shield dimensioning, significantly reduce radiative and convective losses in SMR containment gaps. Figure 7 presents the calculation formula and results in heat loss from the chamber to the ambient air.

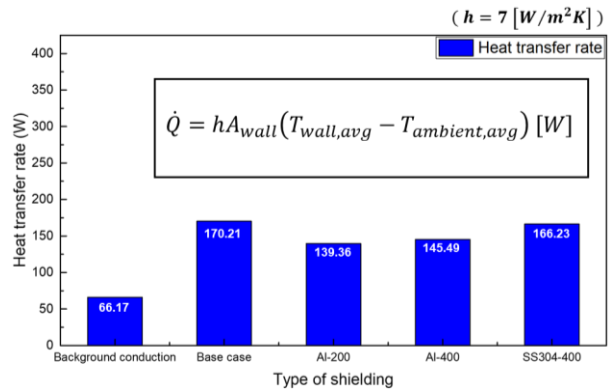


Fig. 7. Calculation formula and calculation results for heat loss from the chamber to the ambient air.

4.2 Numerical Simulation Results

All CFD simulations were run until residuals dropped below 10^{-5} for the turbulence equations (k and ω) and 10^{-6} for continuity, energy, and DO intensity. Heat loss from the chamber's exterior boundary was computed in the CFD model and compared to the experimental data (Table 5). Overall, the CFD consistently overpredicted total heat loss by 13–26%. Discrepancies were attributed to using nominal emissivity values (rather than measured ones), simplified boundary conditions, and potential underestimation of real-world flange or conductive losses.

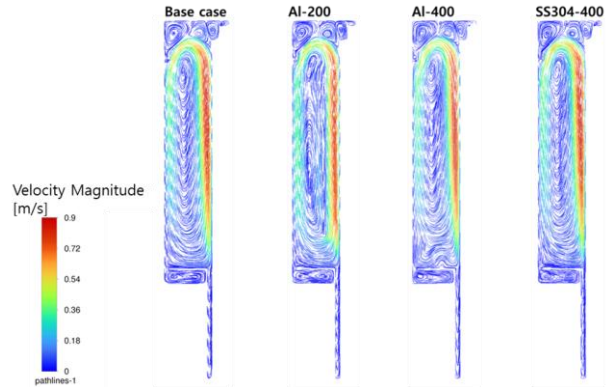


Fig. 9. Streamlines of velocity magnitude inside the chamber for different cases.

Table 5: Comparison of experimental and numerical results: total heat loss for different gap-filling conditions.

	Heater Input (=Total Heat Loss) [W]	
	Experiment [W]	CFD [W] (Error, %)
Background conduction	144.34	166.06 (13.1)
Base case	338.53	448.57 (24.5)
Al-200	289.11	333.63 (13.4)
Al-400	297.03	403.37 (26.4)
SS304-400	327.38	434.75 (24.7)

Figure 8 compares radial temperature profiles, showing that the experimental chamber wall temperatures tended to exceed simulated values. For the Al-200 case, the experiment recorded the lowest chamber temperature, whereas the CFD predicted the highest—likely due to overestimated internal flow patterns (Figure 9). Hence, a transient solver or refined boundary conditions could improve matching.

Further analysis revealed that applying thermal radiation shields (TRSS) significantly reduced radiative flux in the gap region. Table 6 shows the results of CFD calculations for the radiative heat transfer generated in the conductor and the radiative heat transfer that exits through the region of interest. The Base case allowed about 90% of the conductor's radiative output to escape through the area of interest, whereas the Al-400 shield cut that figure to roughly 19%. Similarly, comparing total heat transfer from the area of interest (Table 7) showed that Al-400 maintained the lowest fraction (~40%) among the tested cases.

Table 6: The proportion of radiative heat transfer rate in the area of interest compared to the total radiant heat emitted.

	Total Radiative Heat Loss [W]	Gap to Area of interest [W] (portion, %)
Background conduction	-	-
Base case	232.99	208.45 (89.5 %)
Al-200	144.13	83.62 (58.0 %)
Al-400	199.33	36.78 (18.5 %)
SS304-400	221.84	156.49 (70.5 %)

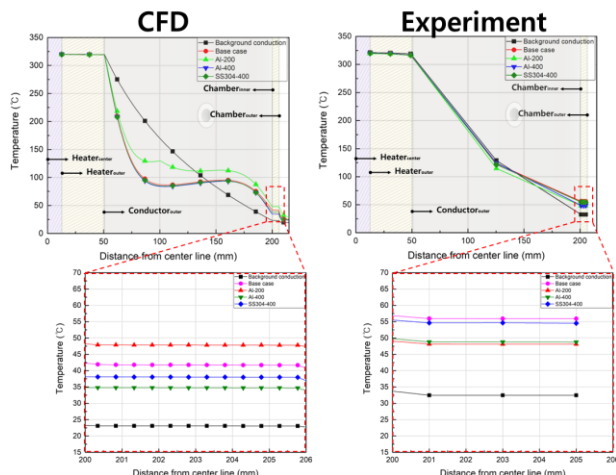


Fig. 8. Comparison of Radial temperature distributions from the center to the chamber wall.

Table 7: Proportion of heat loss in the area of interest relative to total heat loss.

	Total Heat Loss [W]	Area of Interest to External Air [W] (portion, %)
Background conduction	166.06	75.97 (45.7 %)
Base case	448.57	273.45 (61.0 %)
Al-200	333.63	179.87 (53.9 %)
Al-400	403.37	161.46 (40.0 %)
SS304-400	434.75	232.98 (53.6 %)

In conclusion, while CFD captured the overall trends—lower emissivity shields reduced radiative losses more effectively—using experimentally derived emissivities and accounting for secondary conduction paths would further refine the model. A transient approach for the enclosure flow might also resolve the overestimation of velocity magnitudes, enhancing predictive accuracy for SMR applications.

5. Conclusions

This study confirmed that installing a Thermal Radiation Shield (TRS) in a vacuum environment can reduce total heat loss by around 12% compared to an unshielded Base case, with an aluminum TRS at 400 mm diameter (Al-400) delivering the greatest benefit. For an i-SMR, such a reduction corresponds to roughly 75 kW less heat loss, potentially improving reactor efficiency by lowering its average temperature.

The smaller reduction observed here versus a prior computational study (70%) likely stems from differences in emissivity (our aluminum conductor at 0.18 vs. SA508 at 0.7) and unaccounted heat losses through top/bottom surfaces. Numerical simulations largely supported the experimental data, showing an 80% drop in radiative heat transfer to the chamber wall with Al-400, though overall CFD-predicted heat loss was 13–26% higher than measured. This discrepancy underscores the importance of using experimentally verified material properties and boundary conditions.

Flow patterns inside the near-vacuum chamber—particularly in the Al-200 case—hint at the need for transient CFD models to capture internal circulation accurately. Future work should refine boundary conditions, measure actual emissivity, and account for all heat-loss surfaces in both experiments and simulations, further improving SMR thermal management strategies.

Acknowledgments

This study was sponsored by the Korea Hydro & Nuclear Power Co.'s affiliated Central Research Institute (KHNP-CRI).

This work was supported by the Innovative Small Modular Reactor Development Agency grant funded by the Korea Government (MSIT) (No. RS-2024-00404240).

REFERENCES

- [1] S. Susyadi, H. Tjahjono, and D. T. S. Tjahyani, "Numerical Study on Condensation in Immersed Containment System of Advanced Smr during Uncontrolled Depressurization," *Jurnal Teknologi Reaktor Nuklir Tri Dasa Mega*, vol. 19, no. 3, 2017.
- [2] H. S. Yoo, S. H. Yoo, and E. S. Kim, "Heat transfer enhancement in dry cask storage for nuclear spent fuel using additive high density inert gas," *Annals of Nuclear Energy*, vol. 132, pp. 108-118, 2019.
- [3] G. H. Lee, J. H. Park, B. Jeong, and S. J. Kim, "Analysis of heat-loss mechanisms with various gases associated with the surface emissivity of a metal containment vessel in a water-cooled small modular reactor," *Nuclear Engineering and Technology*, vol. 56, no. 8, pp. 3043-3066, 2024.
- [4] M. F. Modest and S. Mazumder, *Radiative heat transfer*. Academic press, 2021.
- [5] M. Ghane and E. Ghorbani, "Investigation into the UV-Protection of Woven Fabrics Composed of Metallic Weft

Yarns," *Autex Research Journal*, vol. 16, no. 3, pp. 154-159, 2016.